

# 30 T ON TARGET NEUTRINO FACTORY/MUON COLLIDER FRONT-END

J.C. Gallardo, H. Kirk, BNL, Upton, NY 11973, USA

K. McDonald, Princeton University, Joseph Henry Laboratories, Princeton, NJ 08544, USA

D. Neuffer, FNAL, Batavia, IL 60510, USA

The main objective of the study is to investigate the effects of a higher magnetic field on the target. The Neuffer front end consists of

- Target and capture section
- Bunching and rf phase rotation sections
- cooling lattice

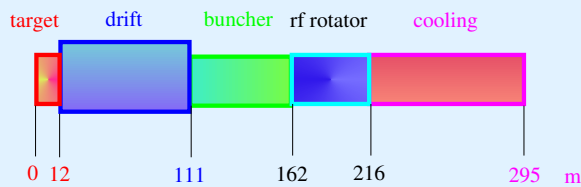


Figure 1: Layout of the Front-End.

## Different Components of the Front-End

- \* **Capture Section:** Hg jet target; 2-3 ns 8 GeV proton (24 GeV). Solenoidal channel: Length  $\approx 12$  m,  $30 (20) \geq B_z \geq 2.6 (1.75)$  T
- \* **Decay Drift:** Length  $\approx 100$  m,  $B_z \approx 2.6 (1.75)$  T
- \* **Adiabatic Bunching:** 27 cavities with 13 different  $\downarrow$  frequencies and changing  $\uparrow$  gradients. Length  $\approx 50$  m,  $B_z = 1.75$  T
  - $333 \leq f \leq 234$  MHz     $5 \leq Grad. \leq 10$  MV/m
- \* **Phase Rotator:** 72 cavities with 15 different  $\downarrow$  frequencies; constant gradient. Length  $\approx 50$  m,  $B_z = 1.75$  T
  - $232 \leq f \leq 201$  MHz     $Grad = 12.5$  MV/m
- \* **Cooling:** Solenoidal FOFO lattice; Length  $\approx 50$  m,  $B_z = \pm 2.8$  T;  $Grad. = 15.25$  MV/m,  $f = 201.25$  MHz

## Bunching and Phase Rotation Region

In the scheme the correlated beam is first adiabatically bunched using a series of rf cavities with decreasing frequencies and increasing gradients. The beam is then phase rotated with a second string of rf cavities with decreasing frequencies and constant gradient. The final rms energy spread in the new design is 10.5%.

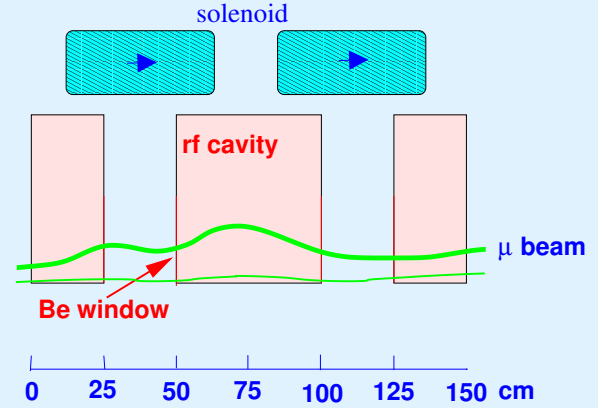


Figure 2: Schematic of 2 cells of the buncher or rotator section.

## Cooling Section

A novel aspect of this design comes from using the windows on the rf cavity as the cooling absorbers. This is possible because the near constant  $\beta$  function does not significantly increase the emittance heating at the window location. The window consists of a 1 cm thickness of LiH with a  $75\mu\text{m}$  layer of Be on the rf cavity field side and,  $25\mu\text{m}$  layer of Be on the opposite side. (The Be will, in turn, have a thin coating of TiN to prevent multipactoring). The alternating 2.8 T solenoidal field is produced with one solenoid per half cell, located between the rf cavities.

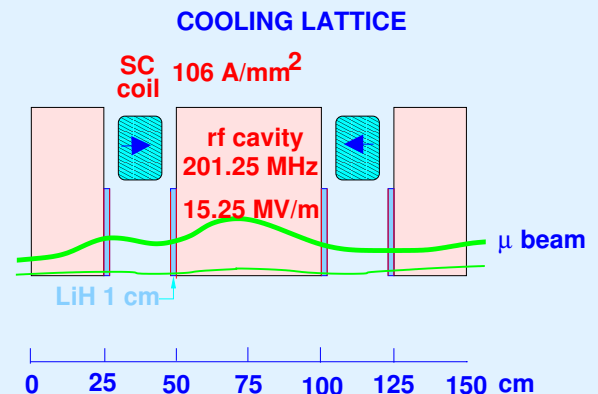


Figure 3: Schematic of one cell of the cooling section. Beta function is constant  $\approx 80$  cm. Windows are absorbers.

## Simulation Performance: 20 T Solenoid on Target

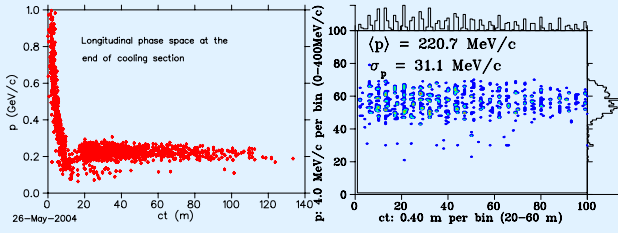


Figure 4: Longitudinal phase space at the end of the channel.

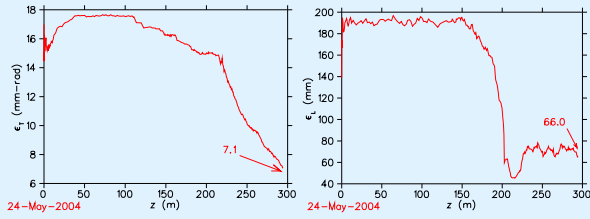


Figure 5: Normalized transverse emittance (left) and longitudinal emittance (right) along the front-end for a momentum cut  $0.1 \le p \le 0.3 \text{ GeV/c}$ .

**Number of  $\mu/p$  in  $A_{\perp}$  and  $A_L$  : Final values are 0.176 with 24 GeV and 0.08 with 8 GeV protons on target.**

Table 1: Table of Results.

$\langle p_z \rangle$ Mean Momentum (MeV/c)	220
rms Energy Spread (MeV)	31
$\epsilon_{\perp}^N$ (mm-rad)	7.1
$\epsilon_{\perp}^{equil.}$ (mm-rad)	5.5
$\epsilon_L^N$ (mm)	66
$A_{\perp}$ (mm-rad)	30
$A_L$ (mm)	150
No. $\mu/p$ in $A_{\perp}$ and $A_L$	0.08

## Simulation Performance: 30 T Solenoid on Target

We use a MARS generated  $\pi$ s file for an optimized target system with 8 GeV proton on Hg. The magnetic field on Target, Capture, Drift is *naively* scaled by a factor of  $\frac{3}{2}$  and the radius of the pipeline is decrease to 25 cm same size as the Be windows in Buncher and Rotator sections.

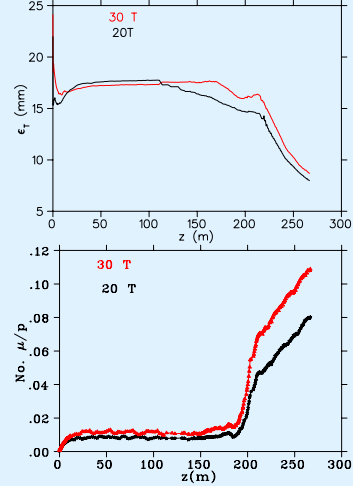


Figure 6: Comparison between 20 and 30 T examples: (top) transverse emittance vs z; (bottom) number of muons per incident proton on target vs z. Final values: for 20 T is 0.08; for 30 T is 0.11.

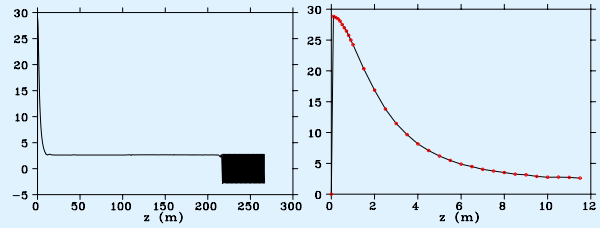


Figure 7: (Left) Magnetic field (T) on the total length of the front end; (Right) magnetic field (T) on the capture region.

In this examples the constant magnetic field on both bunching and rotator sections was  $2.6 \text{ T} (1.75 \times \frac{3}{2})$ . **If we reduce the field to the standard 1.75 T and disregard the lack of matching at the different magnetic field inter-phases, then**

### Suggested Conclusions

- New 8 GeV MARS 15 increases the efficiency of the front-end by  $\approx 30\%$
- For a larger magnetic field on target ( $20\text{ T} \implies 30\text{ T}$ ), the efficiency increases by  $\approx 30\%$ .

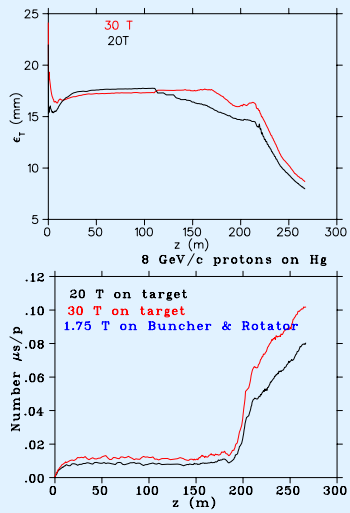


Figure 8: Comparison between 20 and 30 T examples: (top) transverse emittance vs  $z$ ; (bottom) number of  $\mu$ s per incident proton on target vs  $z$ . Final values: for 20 T 0.08; for 30 T 0.10.

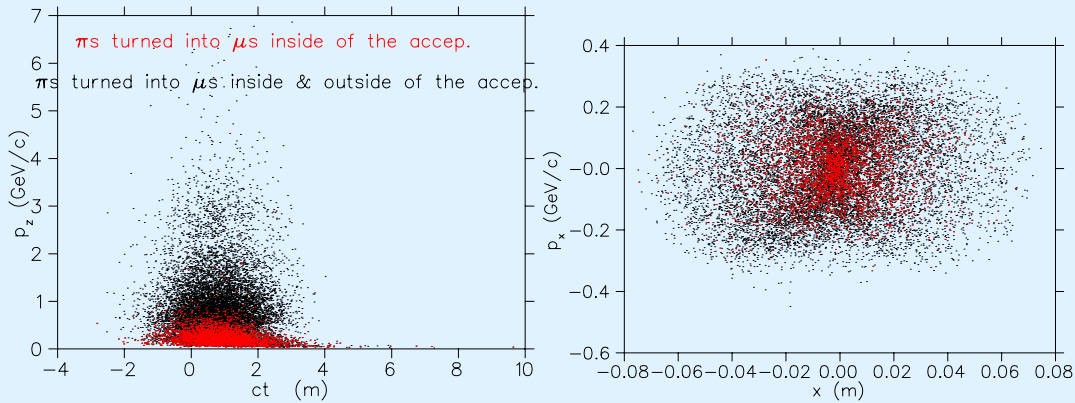


Figure 9: (Left) Longitudinal phase space; (Right) transverse phase space of initial  $\pi$ s. The legend on the left panel it applies also to the right one.

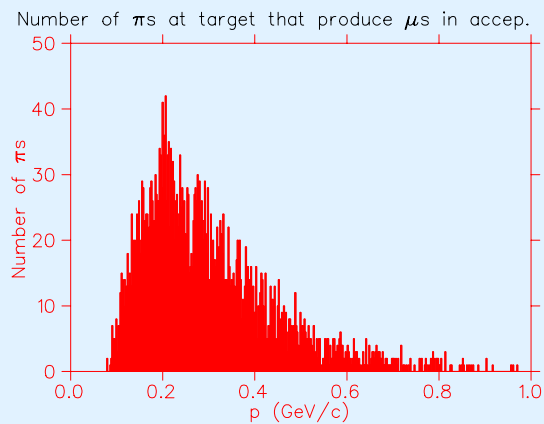


Figure 10: Number of  $\pi$ s on 2.5 MeV/c momentum intervals.